ACTA UNIVERSITATIS AGRICULTURAE ET SILVICULTURAE MENDELIANAE BRUNENSIS

Volume LVIII 12 Number 3, 2010

FRACTAL ANALYSIS FOR OSTEOPOROSIS: A LIKELIHOOD RATIO APPROACH

J. B. Lepschy, M. Stehlík, M. Minárová

Received: April 13, 2010

Abstract

LEPSCHY, J. B., STEHLÍK, M., MINÁROVÁ, M.: *Fractal analysis for osteoporosis: a likelihood ratio approach.* Acta univ. agric. et silvic. Mendel. Brun., 2010, LVIII, No. 3, pp. 119–130

Based on the traditional fractal theory and on the paper of Stehlík, (2009) the range of fractal dimension of osteoporosis vertebras is analysed. First we give an insight into the field of fractals and the usage of fractals in medicine. After this we show how the analytical tool of Stehlík, (2009) may be applied to the osteoporosis vertebras. It turns out that the used method can be applied very well and that it could help with medical diagnosis. Real data example illustrates the methods discussed.

fractals, fractal dimension, deterministic and stochastic models, osteoporosis, cancer, likelihood ratio statistics, chi-square distribution

INTRODUCTION

This paper is about statistical modelling for diagnostics in medicine using fractals. As a lot of human diseases – like osteoporosis vertebras and cancer cells – have a chaotic structure they can be seen as fractals. This field of statistical modelling has a significant importance as it could help to improve the diagnosis of the mentioned diseases. The aim of this paper is to apply an analytical tool which helps to distinguish between healthy and diseased parts in the human body by testing the range of the fractal dimension. Section 1 provides an introduction into the field of fractals. Also the usage of fractals in the field of medicine is briefly mentioned. The results of some already published studies are described. Section 2 introduces the used analytical tool for testing the range of fractal dimension. The analysis is based on the likelihood ratio statistics. Section 3 describes first the data on which the analysis is done. Based on osteoporosis vertebras the descriptive statistics is managed. The testing of the range of fractal dimension is done with different data sets and shows the application of the analytical tool. Last section points out the most important results and outlines the new topics for the further investigation.

FRACTALS IN MEDICINE

The history of fractal began already in the 17th century when Georg Christoph Lichtenberg in the year 1777 fortuitously found a geometric object where all the small parts of the whole looked like the whole itself (Peitgen, Jürgens, Saupe 1992). This was just the beginning of fractals but the phenomenon of fractals raises even today new findings. Originally the word fractal came from the Latin word "fractus" which means to break up or to split up into parts and was characterized by the French mathematician Benoit Mandelbrot. Mandelbrot defines fractal as "a rough or fragmented geometric shape that can be split into parts, each of which is (at least approximately) a reduced-size copy of the whole," (Mandelbrot, 1982). In this subsection we would like to talk about the fractal shapes in the human body and the application of fractals in the field of medicine. We already mentioned at the beginning of the paper the fractal shapes of human lungs. With the help of this knowledge silicosis in the lungs – the so called pulmonary dust – can be detected (http://wwwiaim.ira.uka.de/Teaching/SeminarMedizin/Ausarbeitungen/SS2004/04_Texturbasierte_Segmentierung.pdf). Another example for fractals in the human body is the arterial system: the blood vessels have fractal properties. Sernetz et al. found out, that the arterial system of the kidney is also a fractal with a dimension between 2 and 2.5. There were a lot of studies of different scientists in these fields. They found out, that the growth of the neurons and the vessels of eyes are similar to the DLA (Bunde, Havlin 1994). Further more the fractal geometry can be applied

for the bones structure and vasculature. In this paper we would like to concentrate only on the significance for osteoporosis research.

Fractal Analysis of Osteoporosis

A bone consists of collagen and calcium which are responsible for the flexibility and the strength of a bone. In young years the bones are growing and new bones arise, this process is called formation. At the age of about 30 the bone density and strength of a human reaches the best point. After this the so called resorption of bones begins, which means that the bones are removed and getting weaker and less. Osteoporosis is a disease where the bone mass is low and the bone structure is decreased which means that the resorption is much faster than the formation. Osteoporosis leads to a decrease of the bone stability and causes a higher risk for fractures. For the diagnosis of osteoporosis the bone mineral density (BMD) is measured, mostly with the help of a special form of x-raying, the so called DXA. The resulting t-value can be interpreted as the disease of osteoporosis if the value reaches 2.5 or more (see *http://de.wikipedia.org/wiki/Osteoporose; http://en.wikipedia.org/wiki/Osteoporosis*).

At the moment there exist a lot of studies in this field. In the next step we would like to cite 2 studies for osteoporosis with fractal analysis. Both concentrate on the fractal dimension of the bones and point out the correlation to the bone mineral density (Benhamou et al., 1994; Ishida, et al. 1993).

Benhamou et al. (1994) deals with the different dimensions of bones from 31 persons. 17 persons are osteoporosis patients and the control group consists of 24 persons. The information for the experiment comes from X-ray images. The dimensions are measured by using the box-counting method. The 3 D structure of the bones are represented by a 2 D projection. The basis for the calculation is the fractional Brownian motion (FBM) which is a Gaussian process with the parameter H – the Hurst exponent in the interval [0,1]. The Hurst exponent is directly related to the dimension (D = 2-H) and reveals the roughness. Benhamou et al. (1994) has found that the Hurst exponent is smaller and the dimension is bigger for the osteoporosis patients than for the controlled group. The p-value is very good with the amount of less than 0.0001. Furthermore one can see that there was no correlation with the age of the patients (Benhamou et al., 1994).

The discussion of Ishida et al. (1993) is, inter alia, again the pattern of osteoporosis with fractal dimensions by using the box-counting method. The data is also represented by a 2 D projection. They found out that the dimension of the osteoporosis patients is about 0.306 in contrast to the control group which has a dimension of 1.435 in their study. Furthermore they stated that it is possible to describe the osteoporosis pattern with fractal dimension but it is not possible to classify the direction of the pattern by the dimension.

For the analysis of the data we have applied the method of Stehlík (2009) for testing of the range of fractal dimension. They suppose for testing if a dimension is in a special range a method which is based on the likelihood ratio statistics (Stehlík, 2009). First of all we consider the hypothesis problem.

DESCRIPTION OF THE ANALYSIS

For the analysis of the vertebrae data we have applied the method of Stehlík 2009 for testing of the range of fractal dimension. He supposed for testing whether the dimension is in a special range a method which is based on the likelihood ratio statistics. First of all we consider the hypothesis problem:

1) $\mathbf{H_0}$**:** $\theta = \alpha_0$ **versus H1:** $\theta \neq \alpha_0$ where α_0 is the dimension tested.

   In Stehlík (2009) $x_{11},\ldots,x_{1N}$ is a sample from the Exponential(θ) obtained by the transformation $x_{1i} = \alpha_0 \log||y_{1i}||$ from the single-parameter Pareto. It is proved, that the LR statistics $-\ln\Lambda_N$ of the hypotheses has the following form:

2) $\mathbf{-\ln\Lambda_N = G_N(x_{11}+\ldots+x_{1N}) - G_N(N)}$ with the 2 conditions $\mathbf{x_{1i} = \alpha_0 \log||y_{1i}||}$ and $\mathbf{G_N(x) = x - N\ln(x)}$

   When having the LR Statistics, the corresponding *p*-value is of interest. In the paper they suggested to use the Lambert W function to get the *p*-value. They proposed to use the formula (Stehlík, 2009):

3) $\mathbf{p = 1 - cdf(\tau)}$**, and** $\mathbf{cdf(\tau)}$ **is given in** Stehlík, 2009, where $\tau = -2\ln\Lambda_N$.

   As the Lambert W function is not included in Mathematica we tried to find an easier way to obtain the *p*-value. We found an answer by using the asymptotic of the chi-square distribution. Since we have more observations (Data Set 1 has 79 observations) and it is proved by M. Stehlík (2003) that the asymptotic is working well for such a sample size (see Stehlík, 2003), we decided to use the chi-square asymptotics. As $\tau = -2\ln\Lambda_N$ we just have to double the LR Statistics first and then take one minus the cumulative distribution function of the chi-square distribution of τ with 1 degree of freedom.

THE DATA

3D Surface Anatomy of a Lumbar Vertebra

The physical properties, dimension, magnitude, shape and proportions of the vertebrae vary one by one along whole spine. The morphology of the vertebrae, and of course also the physical properties of their components are closely related to their unique status.

The original investigated vertebra comes from a real human spine (autopsy). It is a scoliotic vertebra with a strong asymmetry in transverse process and with stenosal spinal canal.

The spatial model in the form of IGES file was imported to the final element software ANSYS Multyphysics. A typical computation within the software consists of three basic steps:

- *Preprocessing* – geometry setting up, entity handling, domains stipulation, material library, materials assigning, element type, meshing
- *Solution* – applying loads, running the task
- *Post processing* – results managing, lists, graphs, output files, data handling.

The data for our investigation are accomplished within the first phase.

The model consists of 1 volume, 755 areas, 1510 lines and 758 points. Before the physical investigations on the model some geometric editing and arrangements are inevitable: optimal local and global coordinate system stipulation, rearranging of the characteristic points, adding key points, partition of the initiate volume because of material disparity and material anisotropy.

Data acquiring from the 3D model

We acquire the data needed for the validation from the surface geometry of three parallel cross sections of the vertebra surface (we call it in the paper as data set 2a, 2b and 2c). The first task after the successful model import is to create a suitable coordinate system as the original global coordinate system was generated automatically while scanning the vertebra lying on the pad. While creating an optimal vertebral local coordinate system we have to overmatch the difficulty of having no exact symmetry, no straight line, and no edge neither in the real vertebra nor within the model. Nevertheless, nearly symmetry in the sagittal view, though in the anterior part of the vertebra, can indicate the direction of the further z axis – taking the bottom wall of the vertebral body as the horizontal plane. The local coordinate system origin is posed to the approximate centre of mass of the vertebral body. Also the scaling was used for the purpose of gaining the dimension synchronization with the software units. The flow line of the adjacent vertebral local coordinate systems origins will afterwards create the spinal line. The possibility of several local coordinate systems handling within the one model, naming and using them alternatively, allows us to use i.e. vertebral and spinal system of coordinates, and switch between them as needed.

The data for the validation are acquired by three parallel cross: sections with three cutting planes perpendicular to z axis. The following plane downed by 3 mm from the previous one along the z axis.

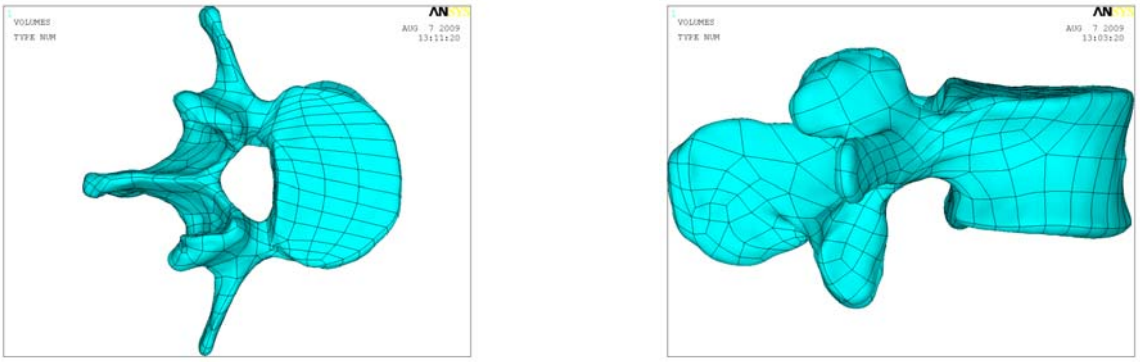

1: *3D model of the real lumbar vertebra. Overhead and side view.*

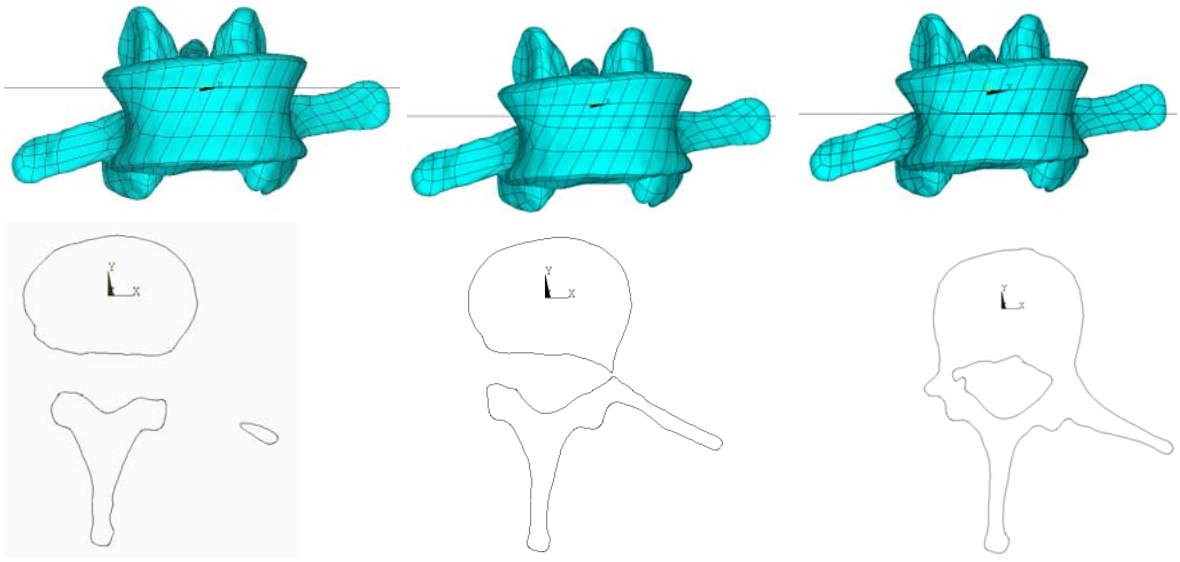

2: *3D model of the real lumbar vertebra. Overhead and side view.*

The records of data set 1 consist of 5 variables where we need 4 of them for the calculations. The data of the vertebras were created by 3 D images as explained above. Thus there are the 3 points – x, y and z – that stands for the coordinates. The 4th variable y_{1i} represents the distance to the zero point of the projection to (x, y)-plane. Data set 2 is of the same vertebras as data set 1. In contrast to the first data set, this data set 2 is not a 3 D image. Therefore we do not need a projection to the (x,y)-plane, as the data is already given in 2 D. It is a cross-section, a so called slice of the vertebras. The data set also consists of 5 variables.

DESCRIPTIVE STATISTICS

Data Set 1

The first data set has 79 observations which are given in metres. We just would like to point out that all the values of x and y are higher than 0 and lower than 1. All values of z are in the interval [–1,0]. We do not work on the 3 D structure but on a 2 D projection of the 3 D image. Therefore it is interesting to have a look at the standard deviation of z. The standard deviation is rather small with a value of 0.00196383. First of all we would like to show a 2 D picture of the vertebras by plotting x against y (Fig. 3).

Next we would like to display how the data looks in 3 D. Therefore we construct a 3 D plot of x, y and z (Fig. 4).

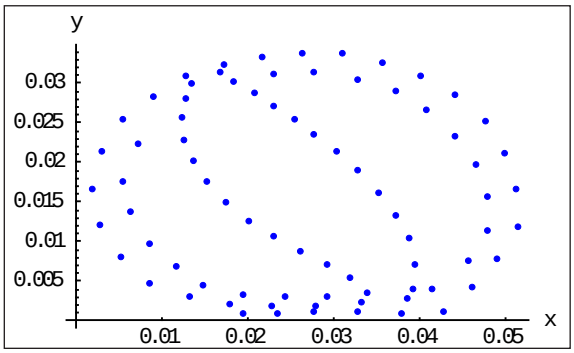

3: *2D image of vertebra (data set 1)*

Data Set 2

Data Set 2 contains 3 different views of the slices. They are all from the same vertebra but they are taken from various heights (= z). Let's call them 2a, 2b and 2c. The following table plots the number of observations and the values of z.

I: *Data set 2 with z and N*

Data	z	Observations N
2a	$z \approx 0$	91
2b	$z \approx 0.003$	111
2c	$z \approx 0.006$	88

In the table one can see, that the most dots are observed with a z of 0.003.

In the following pictures we can see that there are differences in the shapes – depending on the part where the slice was taken from.

TESTING OF THE RANGE OF DIMENSION

Now we would like to test the range of dimension for both data sets as described already before. Starting with the hypothesis, continuing by finding the LR Statistics and the corresponding p-value

1) The hypothesis is H_0: $\theta = \alpha_0$ versus H_1: $\theta \neq \alpha_0$
   So first we have to choose α_0 for our calculations. Considering a dimension in the interval [1,2], it is recommendable to perform the calculations with different α_0. Therefore we regard to vary the values 1 to 2 with steps of 0,1.
2) The Wilks statistics is given by 2) see page 5.
   When first trying to perform these 3 steps – the calculation of the LR Statistics – we may recognize that there is a problem as the positive values of y_{1i} reached negative values when logarithmic them and they could not be logarithmic again. This problem results in the small values of y_{1i} and therefore scaling of the original data should be employed (see Stehlík, 2009). The reason is that Levy flight based approximation of continuous jump probability by Pareto tail works well only for large fractals. Now we could see that this method is not applicable with the osteoporosis data as the method is only working for large fractals. The people providing the data made them in metres which is not practicable for us. As the data has to small scale and the log gets negative we decided to change the scale individually for our data sets.
3) The p-value can be performed by using the cdf of the chi-square distribution.
   1-cdf(chi-square with 1 degree of freedom $(-2\ln x)) = 1 - F(\chi^2_1(\tau))$.

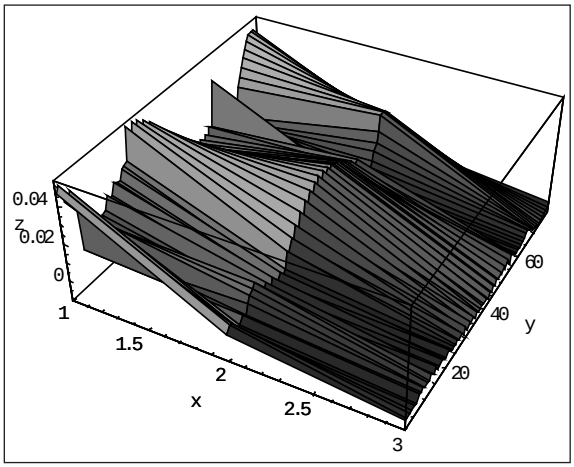

4: *3D image of vertebra (data set 1)*

In this step we select the minimum Wilks statistics of every α_0 between 1 and 2 with respect to c and try to find the corresponding p-value.

Data Set 1

The scaling factor

First we have chosen a scaling factor c of 10, which was not working, so we enlarged the scaling factor to 100 – which means that the data has now changed

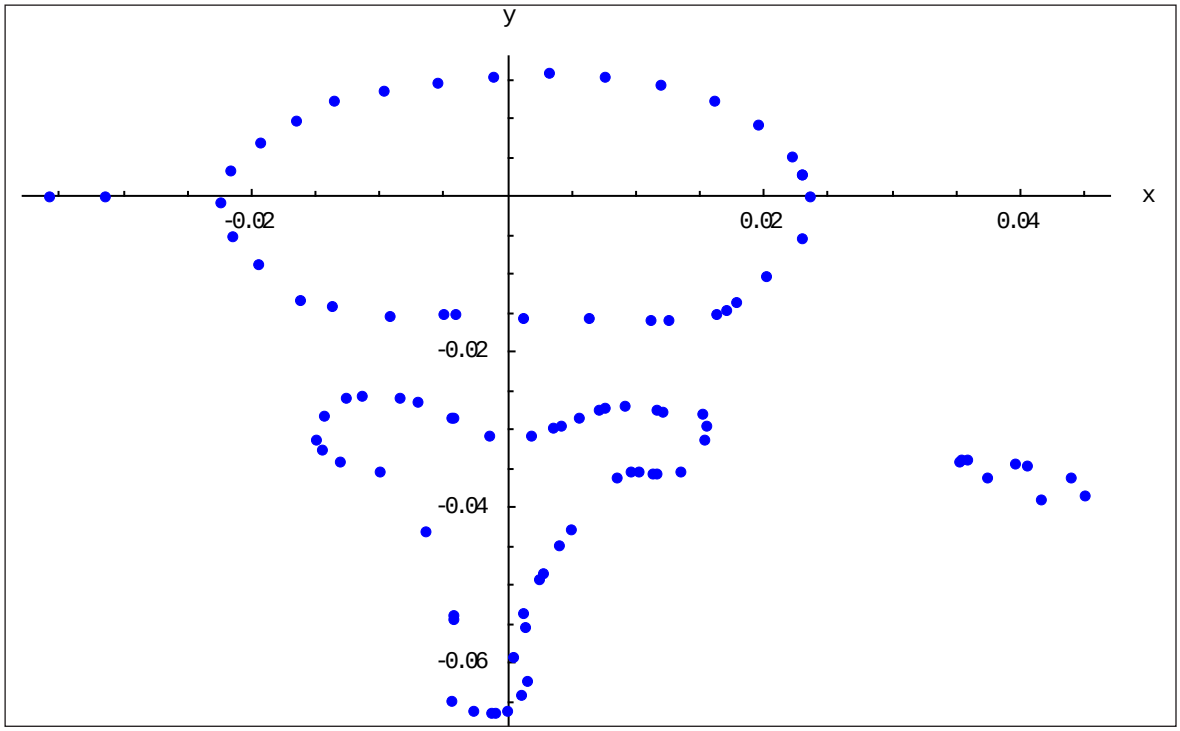

5: *2 D image of vertebra (data set 2a)*

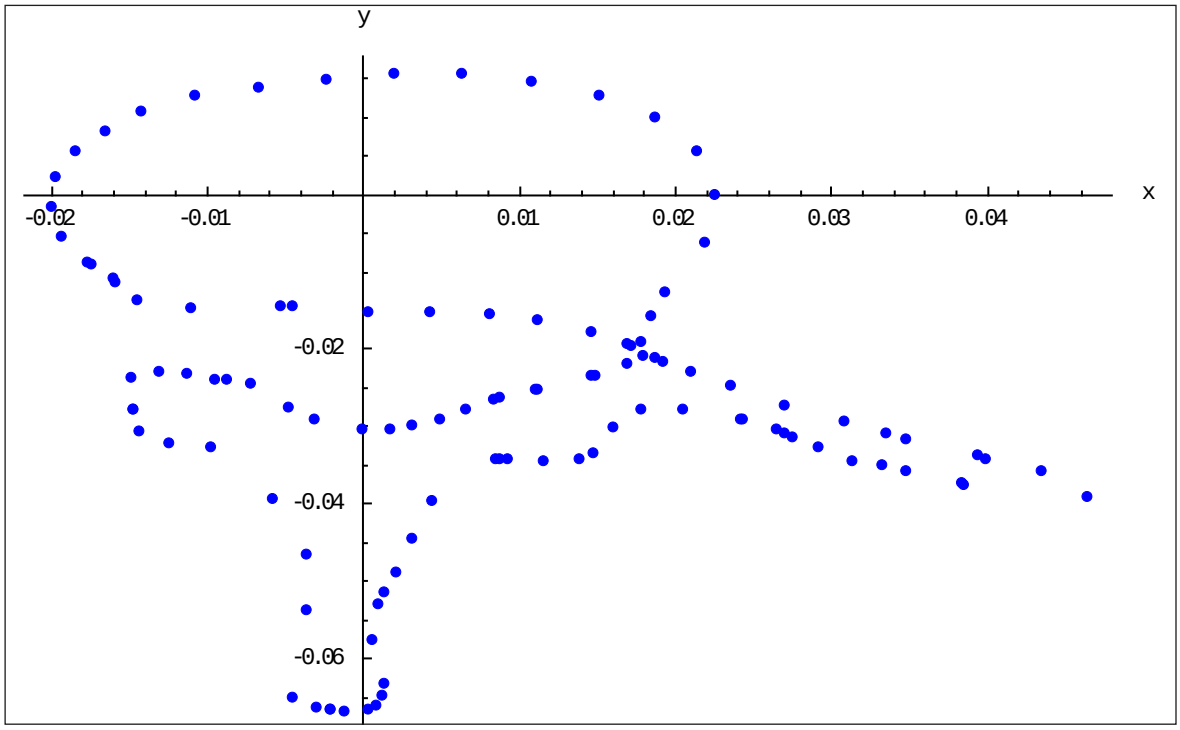

6: *2 D image of vertebra (data set 2b)*

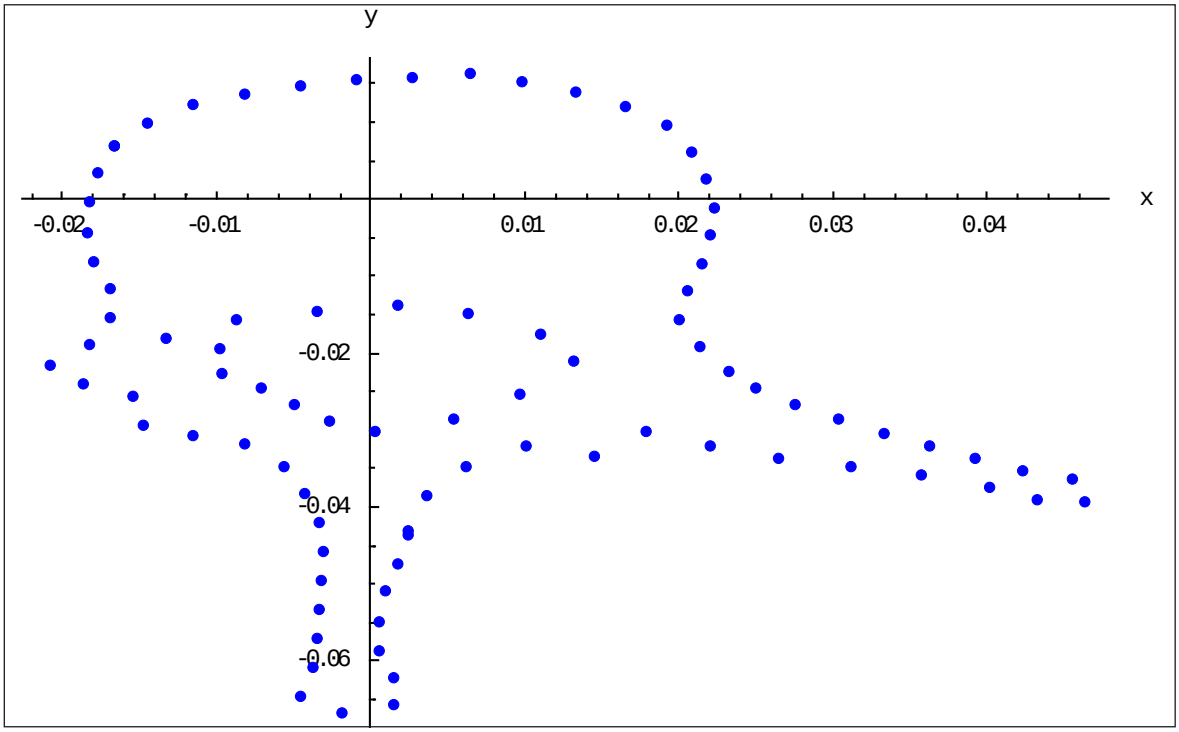

7: *2 D image of vertebra (data set 2c)*

into cm, and it worked. After this we had to find out the minimum scaling factor c where the model worked and found the minimum value for c is 33. When repeating this with different α_0 we found out that the minimum scaling factor stays the same for all α_0. Before calculating all Wilks statistics by varying α_0 and c, we would like to illustrate the calculation.

The results

Starting with $\alpha_0 = 1$ we receive 67 values for the Wilks statistics. We just pick out some of them, the c values in the table are in the interval [33,100] starting at 33 with steps – except the first – of 10. When looking at the results for $\alpha_0 = 1$ one can see that the minimum c value of 33 yields a Wilks statistics of about 218 and only about 0.637 for a c of 100. At the first moment, the Wilks statistics looks as if it is mostly decreasing with a higher amount of c but we will see that this can not be confirmed later.

II: *Wilks statistics, $\alpha_0 = 1$ (data set 1)*

c	$\alpha_0 = 1$
33	218.255
40	59.086
50	20.689
60	7.667
70	2.344
80	0.346
90	0.028
100	0.637

The graph (Fig. 8) demonstrates the Wilks statistics for all integer values of c from 33 to 100.

When looking at the data with other α_0 values than 1, we recognize that the Wilks statistics are only decreasing at the beginning and they are increasing again later. It depends on the selected α_0 whether the values are increasing sooner or later. The following graph shows well this effect.

In the graph (Fig. 9) the turquoise structure is the same as we have seen before with $\alpha_0 = 1$. In contrast to that the green curve ($\alpha_0 = 1.5$) starts increasing earlier and rises to higher values. The blue curve

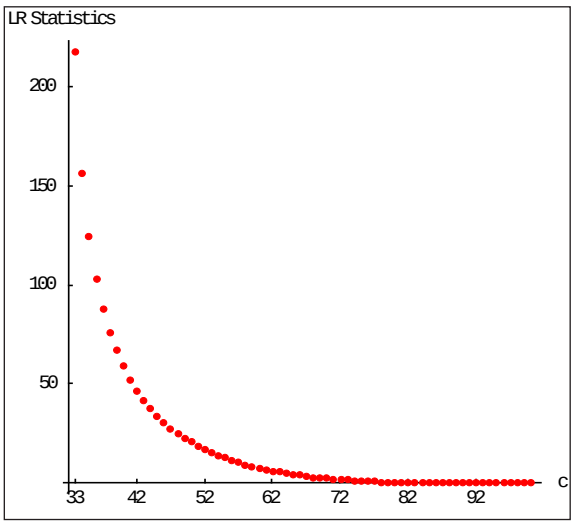

8: *Graph demonstrating the Wilks statistics for integer values of c from 33 to 100*

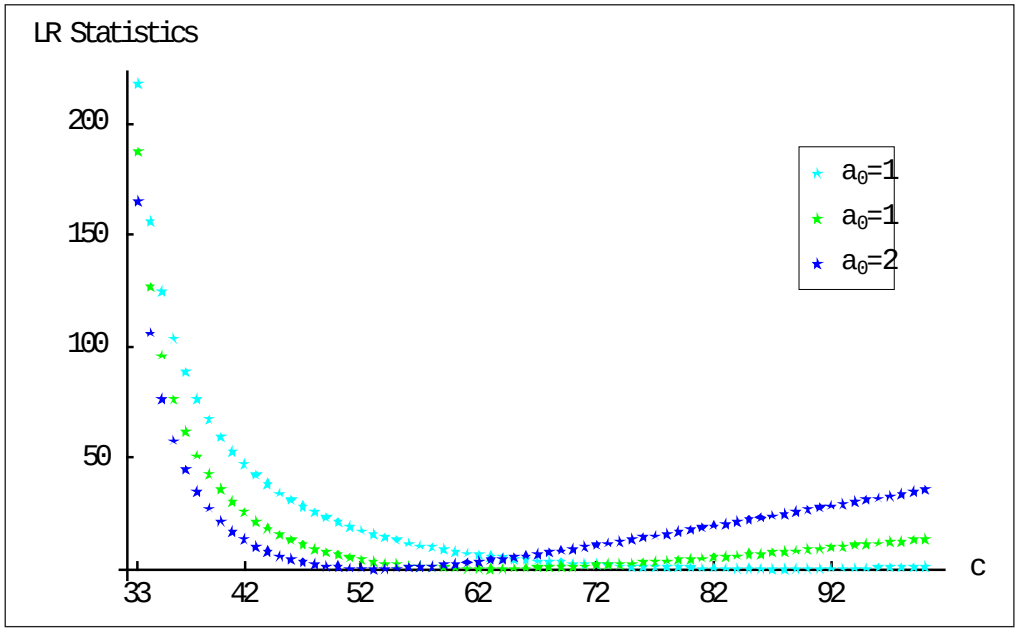

9: *Wilks statistics for α_0 = 1, 1.5 and 2 with different scaling factors (data set 1)*

(α_0 = 2) rises even earlier and higher than the green one. All in all the slope of the curve depends on the α_0 value and the curve is increasing earlier and higher with a larger value of α_0 in our model.

As already mentioned before our next step is to find out at which scaling factor c the Likelihood Ratio gets minimized. When having computed the minimum value with respective to *c*, which is in the interval [33,100], we have to test it for the *p*-value. The next table displays the respective minimum LR with the corresponding scaling factor and *p*-value. E.g. for α_0 = 1 the minimum is reached with the scaling factor of 88 – the LR is 0.000836301.

The *p*-value shows where the dimension is most probably – the higher the *p*-value the likelier the dimension. The smallest value is reached at a dimension of 1.1 with a *p*-value < 0.998.

Excursus: Practical Example

In practice we typically get the specified value for α_0, e.g. in (Benhamou et al., 1994) of 1.5 ± 0.052 for the controlled group and 1.599 ± 0.065 for the osteoporosis group.

III: *Wilks statistics, α_0 = 1, 1.5 and 2 (data set 1)*

c	α_0 = 1	α_0 = 1,5	α_0 = 2
33	218.255	187.163	165.375
40	59.086	35.593	21.404
50	20.689	6.009	0.634
60	7.667	0.189	2.016
70	2.344	0.955	8.871
80	0.346	4.232	17.422
90	0.028	8.566	26.410
100	0.637	13.337	35.342

IV: *Minimum Wilks statistics for different α_0 (data set 1)*

α_0	Minimum LR	c	*p*-value
1	8.36301×10^{-4}	88	0.967378
1,1	2.05348×10^{-6}	80	0.998383
1,2	2.27126×10^{-4}	74	0.982996
1,3	2.83571×10^{-3}	70	0.939969
1,4	5.38503×10^{-4}	66	0.97382
1,5	1.23827×10^{-3}	63	0.96031
1,6	1.16208×10^{-3}	60	0.961549
1,7	3.09707×10^{-5}	58	0.99372
1,8	1.10431×10^{-3}	56	0.962517
1,9	9.6956×10^{-3}	55	0.889251
2	9.41044×10^{-4}	53	0.965396

Conclusion

It is not surprising that the *p*-values are all close to 1 due to the fact that only the points from the boundaries are observed and not the whole. The *p*-value of <0.998 at the scaling factor 80 and a dimension of 1.1 is very remarkable. At this point it would be interesting to measure the dimension on all points – not only on the boundaries, with the Box-Counting method and to compare how stable this method is. This approach will be worth further investigation.

Data Set 2

The scaling factor

The interval for the potential scaling factor c is not the same for all 3 slices. We decided to use the same upper boundary of the interval as we had in data set 1. In the table there are the feasible intervals for each data.

V: *Interval for the scaling factor c*

Data	Interval
2a	[32,100]
2b	[33,100]
2c	[42,100]

The results

Again we are having a look at the LR Statistics for specific α_0 and *c* values. The first table shows the data 2a, where the interval begins with the scaling factor 32.

VI: *Wilks statistics, $\alpha_0 = 1, 1.5$ and 2 (data set 2a)*

c	$\alpha_0 = 1$	$\alpha_0 = 1.5$	$\alpha_0 = 2$
32	537.510	500.658	474.525
40	65.484	38.785	22.805
50	22.917	6.372	0.544
60	8.396	0.146	2.614
70	2.495	1.258	10.740
80	0.330	5.169	20.727
90	0.055	10.253	31.170
100	0.821	15.814	41.525

One can see that the Wilks statistics have the same shape as in data set 1 – they are increasing at the beginning and decreasing at a special *c*-value. E.g. for $\alpha_0 = 1$ the minimum Wilks statistics will be at a scaling factor around 90 and for $\alpha_0 = 1.5$ about 60. We can see the minimum values later.

The next table shows the same as the table before but with the data 2b. The distribution of the values looks similar to the data 2a. The Wilks statistics is smaller at the first scaling factor, but then they are higher in data 2b than in 2a.

VII: *Wilks statistics, $\alpha_0 = 1, 1.5$ and 2 (data set 2b)*

c	$\alpha_0 = 1$	$\alpha_0 = 1.5$	$\alpha_0 = 2$
33	287.0490	243.6240	213.2740
40	81.1421	48.3944	28.7207
50	28.4048	8.0416	0.7523
60	10.456	0.2116	3.0411
70	3.1437	1.4546	12.8395
80	0.4353	6.1573	24.9532
90	0.0550	12.3139	37.6468
100	0.9577	19.0641	50.2444

Last but not least we have done the same with data set 2c and we notice that also these values looks similar concerning the distribution.

VIII: *Wilks statistics, $\alpha_0 = 1, 1.5$ and 2 (data set 2c)*

c	$\alpha_0 = 1$	$\alpha_0 = 1.5$	$\alpha_0 = 2$
42	369.9800	334.5420	309.4690
50	78.7917	51.0254	33.6239
60	33.2431	13.4988	4.1195
70	15.6043	2.6427	0.0460
80	7.1146	0.02837	3.3071
90	2.8219	0.9182	9.3793
100	0.7758	3.5080	16.6050

The next graphs display the Wilks statistics for different scaling factors of the corresponding interval. Again we have chosen $\alpha_0 = 1$, 1.5 and 2. As expected the shapes of the curves look similar to each other.

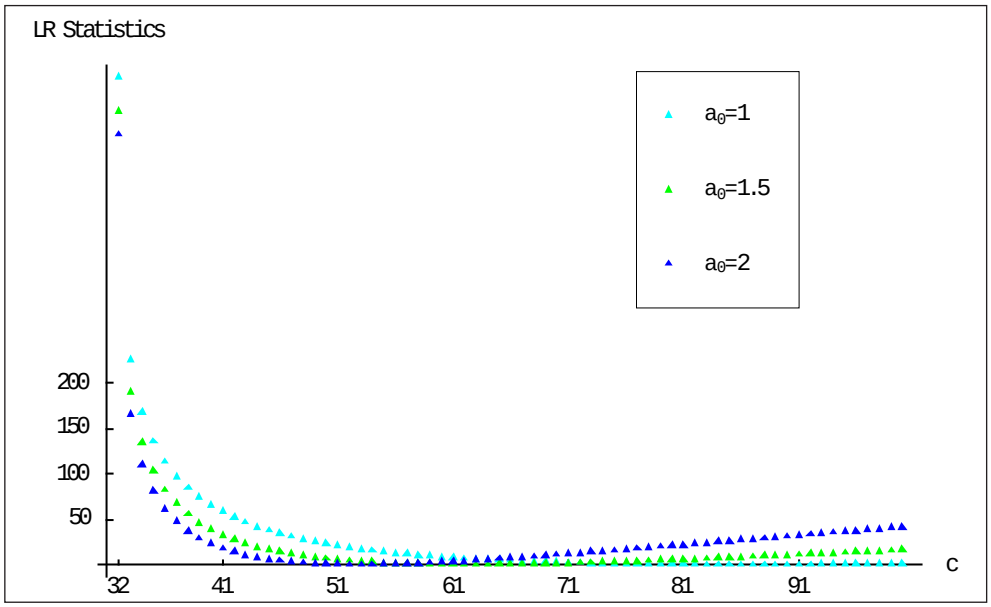

10: *Wilks statistics for $\alpha_0 = 1, 1.5, 2$ with different scaling factors (data set 2a)*

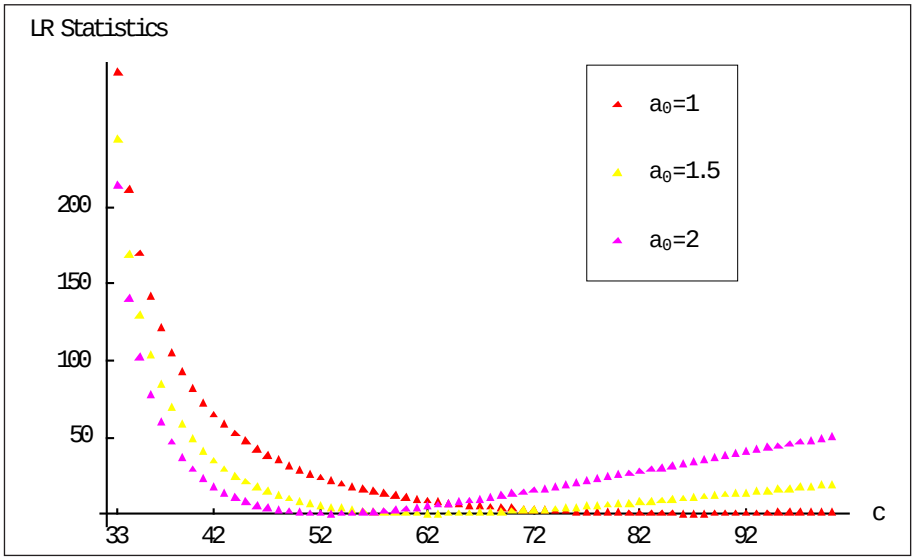

11: *Wilks statistics for α_0 = 1, 1.5, 2 with different scaling factors (data set 2b)*

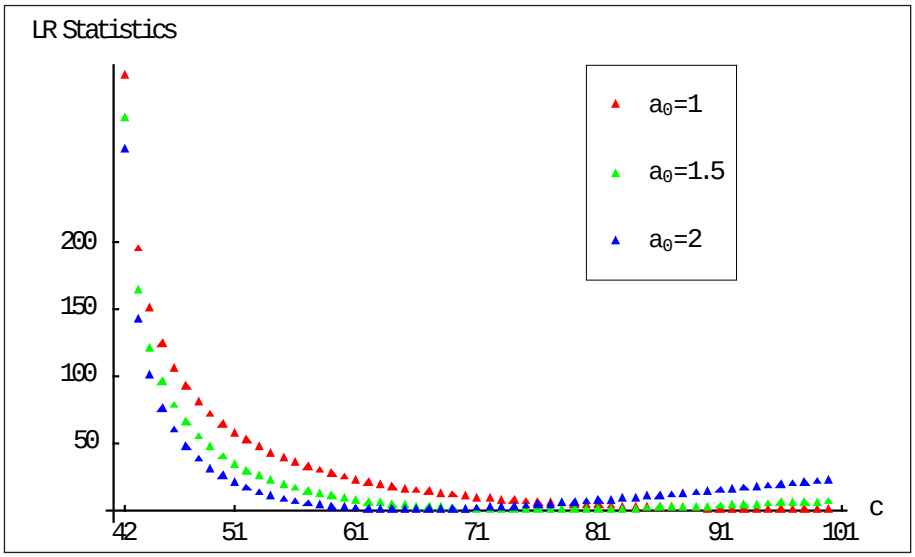

12: *Wilks statistics for α_0 = 1, 1.5, 2 with different scaling factors (data set 2c)*

IX: *Minimum of Wilks statistics for different α_0 (data set 2a, 2b, 2c)*

	Data set 2a			Data set 2b			Data set 2c		
α_0	Minimum of Wilks statistics	c	*p*-value	Minimum of Wilks statistics	c	*p*-value	Minimum of Wilks statistics	c	*p*-value
1	6.26916×10^{-5}	87	0.991066	2.42723×10^{-4}	87	0.982422	3.04708×10^{-2}	100	0.805014
1,1	1.10581×10^{-3}	79	0.963308	1.63146×10^{-3}	80	0.954448	1.46927×10^{-3}	94	0.956769
1,2	2.34583×10^{-3}	74	0.945391	5.96006×10^{-4}	74	0.972458	6.01541×10^{-4}	88	0.972331
1,3	1.54790×10^{-6}	69	0.998596	9.16803×10^{-4}	69	0.965845	1.24213×10^{-3}	83	0.960248
1,4	1.92195×10^{-3}	65	0.950563	5.87001×10^{-3}	66	0.913717	1.49155×10^{-3}	79	0.956443
1,5	1.87120×10^{-3}	62	0.95122	7.13469×10^{-3}	62	0.904915	1.14966×10^{-6}	76	0.998790
1,6	2.46410×10^{-3}	60	0.944034	2.57282×10^{-4}	60	0.981902	9.63465×10^{-4}	73	0.964987
1,7	7.28352×10^{-3}	58	0.903933	2.82908×10^{-3}	58	0.940039	8.53584×10^{-4}	71	0.967042
1,8	3.75510×10^{-3}	56	0.930941	5.80206×10^{-4}	56	0.972825	1.64225×10^{-3}	69	0.954298
1,9	7.02659×10^{-4}	54	0.970096	5.72988×10^{-3}	54	0.914749	5.99240×10^{-7}	67	0.999127
2	5.55810×10^{-3}	53	0.915859	1.16469×10^{-3}	53	0.961506	8.68447×10^{-3}	65	0.895149

Again we try to find out at which scaling factor c the LR Statistics gets minimized and the respective *p*-value. The table (Table IX) displays the minimum LR Statistic with the corresponding scaling factor and the *p*-value. The shaded cells show the minimum LR Statistics. The values are the best for α_0 = 1.3 in data set 2a, α_0 = 1 in data set 2b and α_0 =1.9 in data set 2c. One can see, that also the *p*-values are the best with this dimensions.

VALIDATION OF THE METHOD

Here we provide some details on validation of the method. By using the deterministic fractal given by Sierpinski-Carpet we conducted a massive validation of the method. The main issues to be emphasized are:

1) method is highly dependent in the good scaling, since asymptotics of the Levy flight jumping probability is employed
2) empirical simulation of the critical values of our test may be in some examples more precise
3) the proper design of sampling points may be crucial, since non-deterministic fractal is not substantially random structure
4) small *p*-values might not be disturbing, since we are interesting in having the good "decision rule". In particular, small *p*-values and power functions values may be caused by porus media character of underlying medium
5) As the method just works with higher density we conclude, that the *p*-values are getting better with a higher number of steps of the Sierpinski-Carpet (e.g. steps = 1000). Furthermore we can see, that this method only works for the boundaries.

CONCLUSION

The aim of this paper was to apply an analytical tool which helps to find out the range of dimension of different healthy and diseased parts in the human body. For the analysis we decided to take an example of osteoporosis to perform the tool. In this paper we analysed the sample points from the human vertebra by using the method of Stehlík (2009) which is based on the likelihood ratio statistics.
We found out, that the scaling is very important. The reason is, that our method is using the asymptotically stable law of continuous jump density. The similar method appears in Filus, J., Filus, L. and Stehlík, M. (2009). However they use the pseudoexponential dependence between the samples. Here we work only on the one sample.
Furthermore we recognized that we can use well chi^2 asymptotics to obtain the *p*-value. As already mentioned in the paper it would be interesting to measure the dimension on all points with the Box-Counting method for comparing how stable this method is. The method works relatively well but there should be more testing and validation. All in all we think there should be done much more research with this approach as it could be employed in the field of medical diagnostics.

SOUHRN

Fraktálna analýza osteoporózy: prístup podielom vierohodnosti

Na základe klasickej teórii fraktálov a článku Stehlík, (2009) sa zaoberáme analýzov fraktálnej dimenzie osteoporotických stavcov. Na začiatku článku približujeme užitočné výsledky z teórie fraktálov a ich použitie v medicíne. Potom ilustrujeme použitie analytického nástroja z Stehlík, (2009) na fraktálnu dimenziu osteoporotických stavcov. Ukazuje sa, že metóda môže slúžiť ako pomocný analytický nástroj pre diagnostiku ostoporózy.

fraktály, fraktálna dimenzia, deterministické a stochastické modely, osteporóza, rakovina, podiel vierohodnosti, chi-kvadrát rozdelenie

Acknowledgement

We acknowledge grants VEGA 1/0269/09, APVV – 0351 – 07.

REFERENCES

ADDISON, P. S., 1997: Fractals and Chaos. An Illustrated Course. Florida: CRC. Press.

BAUER, W. and MACKENZIE, C. D.: (w.y.). Cancer Detection via Determination of Fractal Cell Dimension. USA: Michigan State University.

BAUMANN, G., 2005: Mathematica for Theoretical Physics. New York: Springer-Verlag.

BENHAMOU, C. L. et al., 1994: Changes in Fractal Dimension of Trabecular Bone in Osteoporosis: A preliminary study. In: *Nonnenmacher, T. F., Losa G. A. and Weibel,* E. R., Fractals in Biology and Medicine (292–298). Basel: Birkhäuser.

BUNDE, A. and HAVLIN, S., 1994: Fractals in Science. Berlin: Springer-Verlag.

FILUS, J., FILUS, L. and STEHLÍK, M., 2009: Pseudo-exponential modelling of cancer diagnostic testing. In: *Biometrie und medizinische Informatik Greifswalder Seminar- berichte (ISBN 978-3-8322-7481-8 with Shaker Publ.),* Paper 15, 41–54.

ISHIDA, T. et al., 1993: Trabecular Pattern Analysis Using Fractal Dimension, *Jpn. J. Appl. Phys.* Vol. 32 (Part 1, No. 4), 1867–1871.

MANDELBROT, B. B., 1977: Fractals: Form, Chance and Dimension. San Francisco: Freeman.

MANDELBROT, B. B., 1987: Die fraktale Geometrie der Natur. Basel: Birkhäuser.

PEITGEN, H.-O., JÜRGENS, H. and SAUPE, D., 1992: Bausteine des Chaos. Fraktale. Berlin: Springer-Verlag.

STEHLÍK, M., 2003: Distributions of exact tests in the exponential family. Metrika 2003 57: 156–164.

STEHLÍK, M., 2009: Topological aggregation and dependence structures, Ifas research Report.

Address

Jessica B. Lepschy, Bc., RNDr. Milan Stehlík, Ph.D., Ústav aplikované statistiky, JKU Linz, Freistädter Straße 315, A-4040 Linz a. D., Rakousko, e-mail: jessica.lepschy@gmx.at, Milan.Stehlik@jku.at, RNDr. Mária Minárová, PhD., KMDG, Stavebná fakulta STU, Radlinského 11, 813 68 Bratislava, Slovenská republika, e-mail: minarova@math.sk